BIOCHEMISTRY
including biophysical chemistry & molecular biology

Article

pubs.acs.org/biochemistry

The Coil-to-Helix Transition in IlvN Regulates the Allosteric Control of *Escherichia coli* Acetohydroxyacid Synthase I

N. Megha Karanth and Siddhartha P. Sarma*

Molecular Biophysics Unit, Indian Institute of Science, Bangalore 560012, Karnataka, India

Supporting Information

ABSTRACT: The solution structure of IlvN, the regulatory subunit of *Escherichia coli* acetohydroxyacid synthase I, in the valine-bound form has been determined using high-resolution multidimensional, multinuclear nuclear magnetic resonance (NMR) methods. IlvN in the presence or absence of the effector molecule is present as a 22.5 kDa dimeric molecule. The ensemble of 20 low-energy structures shows a backbone root-mean-square deviation of 0.73 ± 0.13 Å and a root-mean-square deviation of 1.16 ± 0.13 Å for all heavy atoms. Furthermore, more than 98% of the backbone φ and ψ dihedral angles occupy the allowed and additionally allowed regions of the Ramachandran map, which is indicative of the fact that the structures are of high stereochemical quality. Each protomer exhibits a $\beta\alpha\beta\beta\alpha\beta\alpha$ topology that is a characteristic feature of the ACT domain seen in metabolic enzymes. In the valine-bound form, IlvN exists apparently as a single conformer. In the free form, IlvN exists as a mixture of conformational states that are in intermediate exchange on the NMR time scale. Thus, a large shift in the conformational equilibrium is observed upon going from the free form to the bound form. The structure of the valine-bound form of IlvN was found to be similar to that of the ACT domain of the unliganded form of IlvH. Comparisons of the structures of the unliganded forms of these proteins suggest significant differences. The structural and conformational properties of IlvN determined here have allowed a better understanding of the mechanism of regulation of branched chain amino acid biosynthesis.

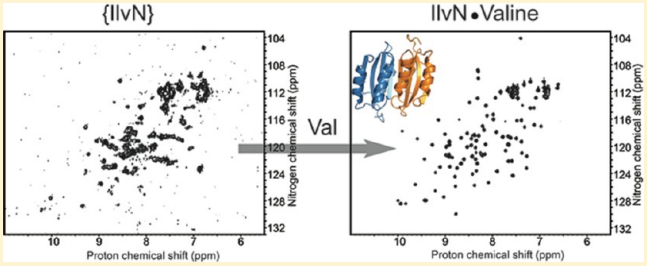

Acetohydroxyacid synthase catalyzes the acyloin-like condensation of two molecules of pyruvate or one molecule of pyruvate and one molecule of 2-ketobutyrate to produce acetolactate or 2-aceto-2-hydroxybutyrate, respectively. This constitutes the first and committed step in the biosynthesis of the branched chain amino acids. This enzyme is found in bacteria, fungi, and plants.[1] The AHAS holoenzyme is a multisubunit enzyme that consists of large catalytic subunits (CSUs) and small regulatory subunits (RSUs) and requires TPP, FAD, and Mg^{2+} for activity.[2,3] Enterobacteria are unique, in that they possess three isoforms of this enzyme, viz., AHAS I, AHAS II, and AHAS III. The polypeptide chains for the CSU and RSU of each of these AHASs are encoded by a pair of genes that are juxtaposed on the same operon. These genes are *ilvBN*, *ilvGM*, and *ilvIH*, where *ilvB*, *ilvG*, and *ilvI* are the genes that encode the CSUs and *ilvN*, *ilvM*, and *ilvH* encode the RSUs.[4−6] Other bacteria have the equivalent of *Escherichia coli* AHAS III. While the CSU from across species is well conserved in sequence and structure, the RSU shows significant variation in sequence and size. In general, the polypeptide chains of the RSU of bacterial AHASs are small and range in size from 85 to 170 amino acids (~9.5 to 17 kDa) and are <25% identical in sequence. On the other hand, the RSUs of fungal and plant AHASs are large and range in size from 300 to 500 amino acids (34 to 50 kDa).[7,8] The role of the RSU is twofold. (1) It serves to activate the CSU. Without the RSU, the CSU retains <15% of the activity of the holoenzyme.[9−11] (2) It binds the end products of this metabolic pathway, viz., the branched chain amino acids, and this results in the inhibition of the enzyme and consequently regulation of the flux in this pathway.[1]

Although the reaction catalyzed by AHAS is a seemingly simple one, the architecture and mechanism of regulation are rather complex. The enzymatic and kinetic properties of *E. coli* AHASs, including those mutant proteins that confer resistance to feedback inhibition, have been extensively studied.[12−17] The kinetic and enzymatic properties of the yeast and *Arabidopsis thaliana* AHAS have also been reported.[7,8] In the case of *E. coli* AHASs, AHAS I is completely inhibited by valine, AHAS III is only partially inhibited, and AHAS II is insensitive to inhibition by valine. Recently, it has also been shown that the valine insensitive RSU of AHAS II is able to activate the CSU of AHAS I and AHAS III.[18] Indeed, the N-terminal domain of IlvH alone can activate IlvB but is devoid of the regulatory function.[13] Thus, the structure of the RSU and the structural interactions between the RSU and CSU and that between RSU and the branched chain amino acids are critical to the functioning of this enzyme.

Detailed X-ray crystallographic studies of CSUs from yeast[19] and *Arabidopsis*[20] have shown that the structure of this subunit is well-conserved. Several structures have been determined of the

Received: October 17, 2012
Revised: December 3, 2012
Published: December 3, 2012

CSU from these organisms, as well as those of the CSU in complex with different chemical classes of herbicides.[20−23] The crystal structures of the yeast and *A. thaliana* CSUs have shown that these molecules exist as dimers and tetramers, respectively. In both structures, the individual subunits are folded into three distinct domains (α, β, and γ). The cofactor, TPP, is bound at the dimer interface to the α- and γ-domains from individual subunits. The β-domain binds FAD. There are no structures available for the AHAS holoenzyme from any species.

Of the three AHAS isozymes found in enterobacteria, structural information is available only for the RSU of AHAS III, viz., IlvH.[14] Structures of homologous RSUs from other bacterial species such *Nitrosomonas europaea* AHAS and *Thermotoga maritima* AHAS have also been determined.[24] These structures show that the polypeptide chain is folded into two distinct domains, both of which have a ferrodoxin-like topology. It is important to note that these structures have been determined for the protein molecules in the absence of their physiological regulators, viz., isoleucine, leucine, and valine. The N-terminal domain of the RSU, often termed the ACT domain, binds to these regulators and allosterically modulates the activity of this enzyme.[25−27]

We have initiated structural studies of *E. coli* AHAS I, with the aim of determining the structure of IlvN, the RSU of AHAS I. Our interest lies in determining the structural basis for the interaction between the CSU and RSU of AHAS, leading to activation of the holoenzyme and the structural basis for the allosteric feedback regulation by the branched chain amino acids. Using the CSU and RSU of AHAS I as a model system, we had previously shown that it is the FAD binding domain of IlvB that interacts with the RSU.[28] Here we report the solution structure of IlvN in its valine-bound form. The structure has been determined using high-resolution, multinuclear, multidimensional nuclear magnetic resonance (NMR) methods. The interaction between IlvN and the effector molecules and the accompanying structural changes have been probed using solution NMR spectroscopy and other biophysical methods. The results of these studies are presented below.

MATERIALS AND METHODS

Protein Expression and Purification. Cloning, expression, and purification of IlvN have been described previously.[29] Uniformly ^{13}C- and ^{15}N-enriched or ^{15}N-enriched samples of IlvN were prepared by growing cells in M9 medium containing [$^{13}C_6$]glucose and $^{15}NH_4Cl$ as the sole sources of carbon and nitrogen, respectively, or $^{15}NH_4Cl$ as the sole source of nitrogen.

Gel Filtration Studies. Gel filtration studies were conducted on GE Healthcare Sephacryl S-100 or Sephadex S-75, 26/70 columns, attached to an AKTA Basic FPLC system. Protein samples were eluted from the column using a 20 mM potassium phosphate buffer (pH 7.0) containing 20 mM NaCl, 1 mM EDTA, and 0.01% sodium azide using a flow rate of 1 mL/min. The oligomeric state of IlvN in the presence of valine was studied by inclusion of valine, at a concentration of 5 mM, in elution buffer. The molecular weight was estimated by comparison of elution volume to those of proteins of known molecular weights.

Circular Dichroism Studies. Circular dichroism (CD) spectra were recorded on a JASCO-715 spectropolarimeter over a wavelength range from 250 to 200 nm at a scan speed of 20 nm/min. CD spectra were recorded on samples of IlvN dissolved in 20 mM phosphate buffer (pH 7.0) containing 20 mM NaCl, 1 mM EDTA, and 0.01% sodium azide, using a 1 mm path length cuvette, and the data were averaged over three scans.

Mass Spectrometry. Electrospray ionization mass spectra were recorded on a Bruker Daltonics Ultraflex mass spectrometer. The samples were infused into the mass spectrometer through a reverse phase C18 column by application of gradient elution using a binary solvent system (solvent A, 0.1% trifluoroacetic acid in water; solvent B, 0.1% trifluoroacetic acid in acetonitrile) at a flow rate of 1.0 mL/min. Chemical modification (alkylation) of IlvN in the absence of ligands was conducted by treating IlvN (1.5 μM) with 4 mM iodoacetamide in 40 mM ammonium bicarbonate (pH 8.0) for 5 min in the dark and immediately loaded onto the HPLC column. In the case of chemical modification reactions in the presence of ligand, the protein samples were first incubated with either 5 mM valine or 10 mM isoleucine for 5 min at 37 °C, prior to the alkylation procedure described above.

NMR Spectroscopy. *Sample Preparation.* Isotopically enriched samples of IlvN for solution NMR studies were prepared in 20 mM potassium phosphate buffer (pH 7.0) (90% H_2O/10% D_2O mixture or 100% D_2O), containing 20 mM NaCl, 1 mM EDTA, and 0.01% sodium azide (pH 7.0). No pH correction was made for isotope effects. Protein sample concentrations ranged from 0.1 to 0.5 mM. NMR samples containing valine or isoleucine were prepared by addition of either valine or isoleucine to a final concentration of 5 or 10 mM, respectively. Samples containing valine, isoleucine, or leucine shall henceforth be termed IlvN-V, IlvN-I, or IlvN-L, respectively.

Data Acquisition. NMR data sets were acquired using either an Agilent 600 MHz spectrometer or a Bruker Avance 700 MHz spectrometer. The Agilent 600 MHz NMR spectrometer was equipped with a triple-resonance (z-axis) pulsed field gradient probe, and the Bruker Avance 700 MHz spectrometer was equipped with a room-temperature triple-resonance probe and a cryogenically cooled triple-resonance probe. Spectra were recorded at 303 K. Chemical shifts were referenced to external DSS. Solvent suppression in the case of ^{15}N-edited NMR experiments was achieved using the WATERGATE[30] pulse scheme. In the case of ^{13}C-edited experiments, solvent suppression was achieved using trim pulses.

All two-dimensional ^{1}H−^{15}N[31] and ^{1}H−^{13}C HSQC[32] spectra were recorded using proton spectral widths of 10000 Hz (at 600 and 700 MHz) in the acquired dimensions. ^{15}N chemical shifts were sampled over spectral widths of 1824 Hz (at 600 MHz) and 2128 Hz (at 700 MHz). ^{13}C chemical shifts were sampled over a spectral width of 10914 Hz (at 700 MHz).

Three-dimensional (3D) ^{15}N-edited ^{1}H−^{1}H NOESY[33] spectra (mixing times, τ_m, of 120 and 175 ms) were recorded on ^{15}N-enriched samples of IlvN-V. Proton spectral widths of 10000 Hz (at 700 MHz) were sampled in the F_3 and F_1 dimensions, while a nitrogen spectral width of 2128 Hz (at 700 MHz) was sampled in the F_2 dimension to yield a final time domain data set that was 1024* (t_3) × 128* (t_1) × 25* (t_2) points in size. Three-dimensional ^{13}C-edited ^{1}H−^{1}H NOESY spectra (mixing time, τ_m, of 150 ms) were recorded on uniformly ^{13}C- and ^{15}N-enriched samples of IlvN-V. Proton spectral widths of 10000 Hz (at 700 MHz) were sampled in F_3 and F_1 dimensions, while a carbon spectral width of 4225 Hz (at 700 MHz) was sampled in the F_2 dimension to yield a final time domain data set that was 1024* (t_3) × 32* (t_2) × 128* (t_1) points in size. Data were acquired in phase sensitive mode, using the States−TPPI or Echo−AntiEcho method of quadrature detection for the indirectly detected dimensions.

dx.doi.org/10.1021/bi301415m | *Biochemistry* 2013, 52, 70−83

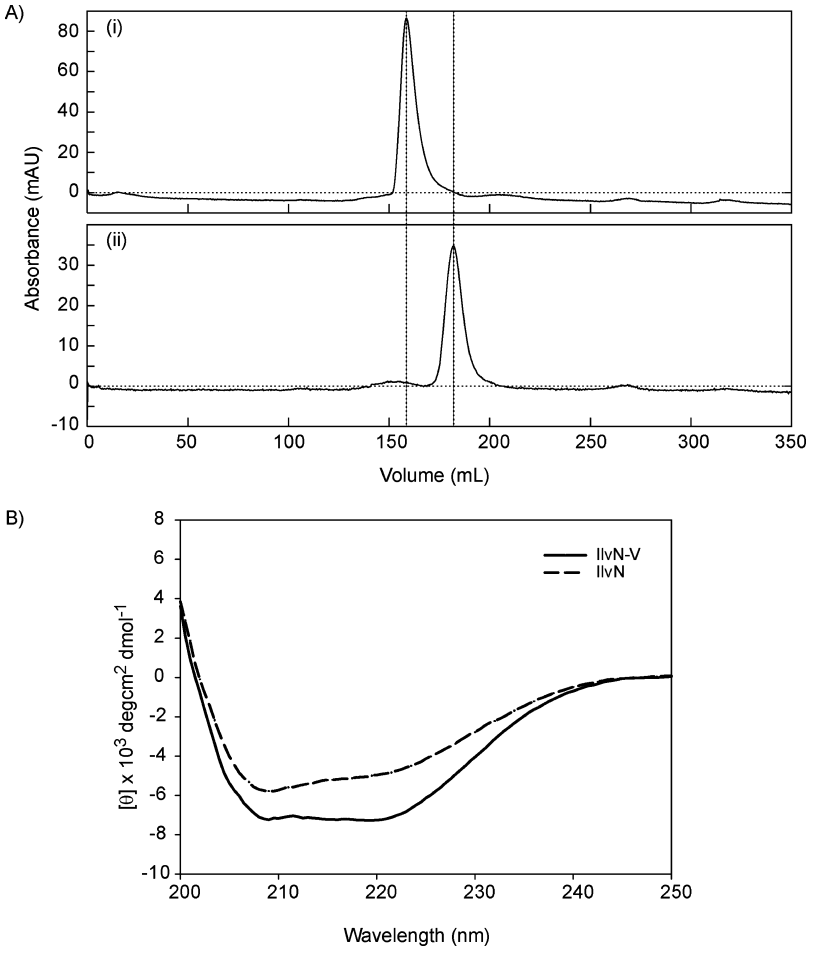

Figure 1. (A) Gel filtration chromatogram showing the elution profiles (i) for IlvN and (ii) and IlvN-V. See the text for details. (B) Circular dichroism spectra of IlvN (25 μM) and IlvN-V (25 μM with 5 mM valine). Comparison of the spectra of the two proteins shows an increase in helical content in the case of IlvN-V.

Hydrogen–Deuterium Exchange Studies. NMR samples of IlvN or IlvN-V were lyophilized and dissolved in 99.9% D_2O prior to data acquisition. Two-dimensional $^{1}H-^{15}N$ HSQC spectra were recorded for a period of 24 h.

Data Processing and Analysis. All data were processed using NMRPipe/NMRDraw[34] data processing software on an Intel personal computer running Suse Linux version 11.1. Time domain data in the directly and indirectly detected dimensions were apodized with a 90° phase-shifted squared sine bell and zero-filled once prior to Fourier transformation and baseline correction. Processed data were analyzed using ANSIG version 3.3[35,36] and the ANALYSIS module in CCPN.[37]

Constraint Generation and Structure Determination. *Distance and Dihedral Angle Restraints.* Correlation peaks that were unambiguously identified between pairs of protons in the ^{15}N-resolved and ^{13}C-resolved NOESY spectra were integrated, and on the basis of integrated intensities, NOEs were classified as strong, medium, weak, and very weak with upper bounds of 2.8, 3.5, 5.0, and 6.0 Å, respectively. H–D exchange studies and knowledge of secondary structure were used to generate the hydrogen bond restraints. Upper distance bounds of 2.2 Å for NH···O bonds and 3.2 Å for N···O bonds were set as restraints between hydrogen bonded donor and acceptor pairs. All distance restraints employed a lower bound of 1.8 Å.

Backbone dihedral angle restraints were predicted by TALOS +,[38] on the basis of experimentally observed backbone $^{1}H^{N}$, $^{1}H^{\alpha}$, $^{13}C^{\alpha}$, $^{13}C'$, and ^{15}N and side chain $^{13}C^{\beta}$ chemical shifts. The predicted ϕ and ψ dihedral angles were incorporated directly as dihedral angle restraints for structure calculation, after allowing for angular variations of ±20°, ±30°, and ±40° for residues in α-helices, β-strands, and loops, respectively.

Structure Solution. Tertiary structures of IlvN-V were calculated with CYANA version 3.0[39] on the basis of experimentally observed NOEs, hydrogen bond distances, and dihedral angle restraints using the torsion angle dynamics protocol. In the process of structure determination, 100 random conformers were subjected to 20000 steps of annealing to obtain an ensemble of 20 structures of acceptable stereochemical quality. These structures were then subjected to refinement in explicit water using CNS version 1.3[40,41] using protocols in PDBStat.[42] Twenty low-energy structures with no NOE violations of >0.5 Å and no dihedral angle violations of >5° and with no van der Waals violations were selected for final analysis. The stereochemical quality of individual structures was assessed using MOLMOL[43] and PSVS.[42] The structure of IlvN-V was then compared with those of homologous proteins using the DALI server.[44] Figures of structures were generated using PyMol.[45]

Amino Acid Binding Studies. *Isothermal Titration Calorimetry.* Equilibrium binding constants for the interaction of valine with IlvN were measured by isothermal titration calorimetry (ITC). ITC experiments were performed on a

dx.doi.org/10.1021/bi301415m | *Biochemistry* 2013, 52, 70–83

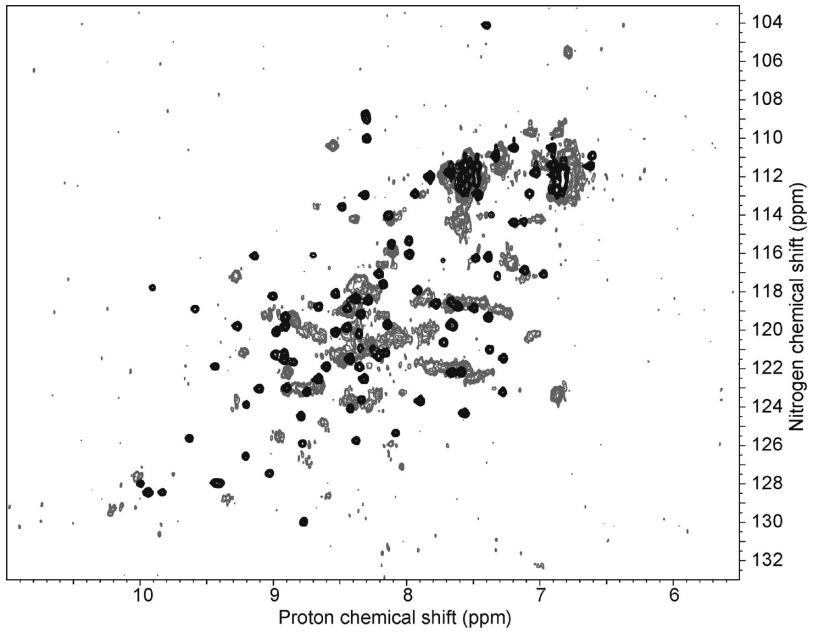

Figure 2. Overlay of the 700 MHz $^{1}H-^{15}N$ HSQC spectra of IlvN (gray) and IlvN-V (black). A significant change in the line widths was observed in going from the valine free state to the valine-bound state. Similar changes were observed upon addition of isoleucine to IlvN (cf., Figure S-2C of the Supporting Information).

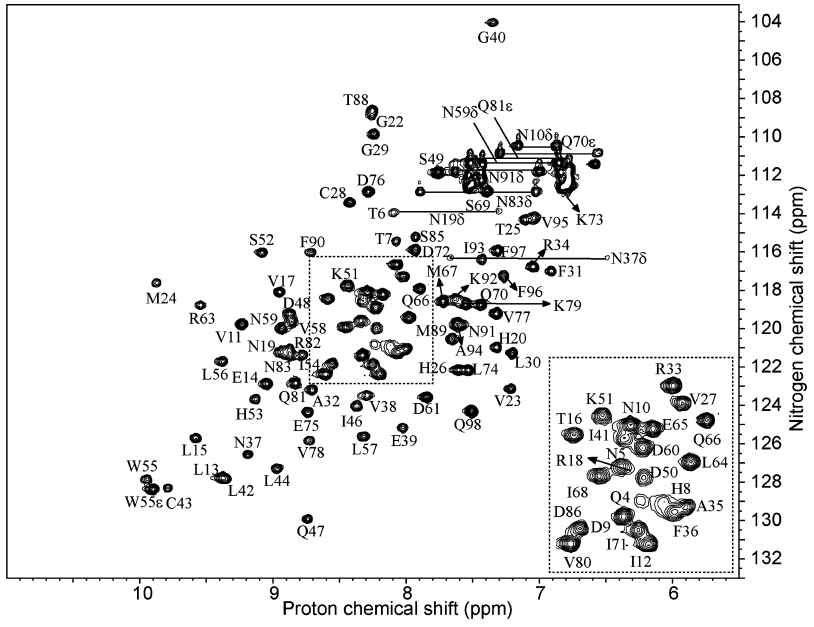

Figure 3. 600 MHz $^{1}H-^{15}N$ HSQC spectrum of IlvN-V showing the sequence specific assignments of IlvN-V. The spectrum was acquired after addition of 5 mM valine to IlvN. The numbering scheme includes two N-terminal residues, which were part of the linker region in the fusion construct. With the exception of M3, Q62, and Q84, all the expected correlation peaks are observed in the spectrum. No conformational heterogeneity can be observed in the spectrum.

MicroCal VP-isothermal titration calorimeter. Aliquots (5 μL) of valine from a stock solution (1.25 mM) in 20 mM potassium phosphate buffer (pH 7.0) containing 20 mM NaCl, 1 mM EDTA, and 0.01% sodium azide (pH 7.0) were injected into the sample cell containing 0.1 mM IlvN in a buffer of the same composition. The temperature was maintained at 25 °C. The data were fit into a one-site binding model and analyzed using MicroCal Origin to obtain the dissociation constant.

Structural Studies of the Interaction of Valine and Isoleucine with IlvN. A competitive binding study was conducted to identify those residues in IlvN that were involved in binding valine or isoleucine. Such a competitive binding method was necessitated by the fact that addition of valine or isoleucine causes abrupt changes in the spectrum of IlvN, making it difficult to follow the progress of a titration reaction. Because the K_d of binding of isoleucine to IlvN was known to be higher,[3] a competition titration was performed wherein valine was added in aliquots to a solution of uniformly ^{15}N-labeled IlvN (0.2 mM) that held saturating quantities of isoleucine (10 mM). The valine concentration was thus continuously increased to a final

dx.doi.org/10.1021/bi301415m | *Biochemistry* 2013, 52, 70−83

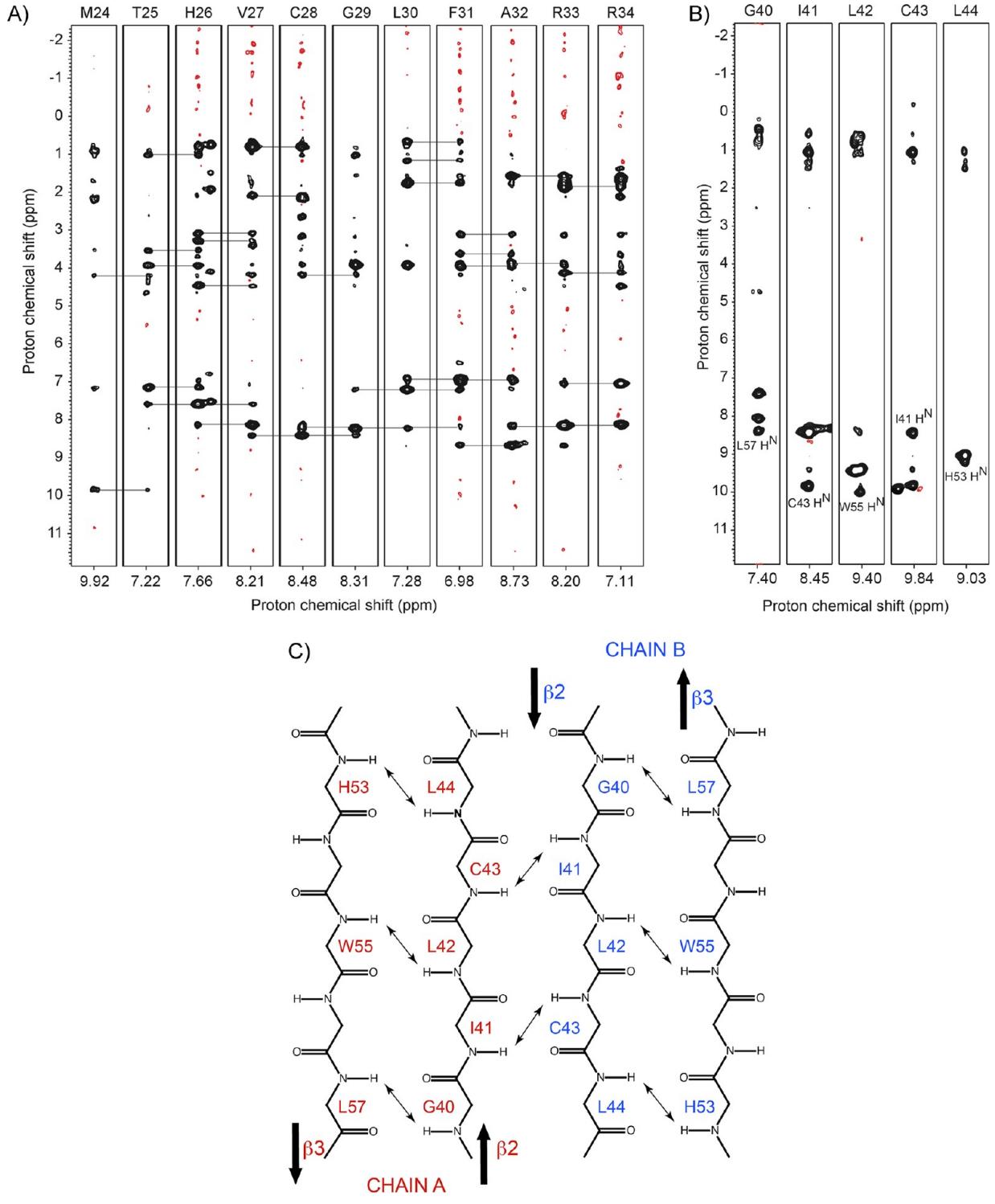

Figure 4. (A) Strip plots from the 3D ^{15}N-edited NOESY-HSQC spectrum of IlvN-V. Contiguous backbone H^N–H^N and H^α–H^N NOEs can be observed for residues 24–34 in the protein. The existence of H^N–H^N NOEs indicates that these residues are present in an α-helical conformation. Side chain–backbone NOEs can also clearly be identified in the spectrum. (B) Representative plot from the 3D ^{15}N-edited NOESY-HSQC spectrum of IlvN-V showing intersubunit NOEs between the backbone H^N–H^N NOEs of I41 and C43. (C) Schematic representation of the H^N–H^N NOEs observed between β2 strands across the dimer interface and the intrasubunit H^N–H^N NOEs between strands β2 and β3.

concentration of 10 mM by the end of the titration studies. After each increment of valine, ^{1}H–^{15}N HSQC spectra were recorded and amide proton–amide nitrogen chemical shift changes were monitored by analysis of these spectra. Backbone amide proton–nitrogen pairs in IlvN that showed chemical shift changes of >0.05 ppm were considered to be interacting with the amino acid.

RESULTS

Solution Properties of IlvN and IlvN-V. Our studies here show that IlvN and IlvN-V exist in conformationally and

dx.doi.org/10.1021/bi301415m | *Biochemistry* 2013, 52, 70–83

Table 1. Experimental Restraints and Structural Statistics for the 20 Lowest-Energy Structures of IlvN-V

no. of experimental restraints	
distance restraints from NOEs	2770
intraresidue	1292
sequential	665
medium-range	312
long-range	463
interchain	38
hydrogen bond distance restraints	144
dihedral angle restraints (φ and ψ)	364
no. of structures in ensemble	20
no. of restraint violations	
no. of NOE violations of >0.5 Å	0
no. of dihedral angle violations of >5°	0
rmsd of atomic positions for residues 10−96 of the ensemble (Å)	
backbone atoms	0.73 ± 0.13
all heavy atoms	1.16 ± 0.13
Ramachandran plot statistics for the ensemble (%)	
most favored	88.4
additionally allowed	10.4
generously allowed	1.2
disallowed	0

structurally distinct ligand free and ligand-bound states. Evidence of this comes from biophysical and NMR studies.

Figure 1A shows the gel filtration chromatography elution profiles for IlvN and IlvN-V. Comparison of elution volumes with those of proteins of known molecular weight (Figure S-1 of the Supporting Information) clearly indicates that IlvN and IlvN-V both exist as dimers. A shift in the elution volume in the case of IlvN-V can be clearly observed, suggesting that there is a decrease in the hydrodynamic radius when the molecule binds valine.

Circular dichroism studies of the proteins show that this decrease in hydrodynamic radius is accompanied by changes in secondary structure. Figure 1B shows an overlay of the CD spectra of IlvN and IlvN-V. The sharpening of troughs at 208 and 222 nm in the case of IlvN-V indicates an overall increase in helicity in the molecule.

The one-dimensional proton and two-dimensional $^{1}H-^{15}N$ correlation spectra of IlvN and IlvN-V (Figure 2) exhibit solution properties characteristic of folded proteins. The one-dimensional spectra of IlvN and IlvN-V, -I, and -L are shown in Figure S-2 of the Supporting Information. The NMR spectra of IlvN show resonances that have broad lines, indicative of a species with a longer rotational correlation time, because of aggregation, or of a molecule that is undergoing significant conformational exchange on the chemical shift time scale. In contrast, the resonance lines manifest in the spectra of IlvN-V show considerable line narrowing in both the upfield and downfield regions. Determination of the dissociation constant for the IlvN−valine complex by NMR was limited by the fact that resonance positions and intensities change abruptly as the valine concentration is increased during a titration study. The dissociation constant was subsequently determined by isothermal titration calorimetry and was found to be 20.12 ± 2.14 μM (Figure S-3 of the Supporting Information). Thus, valine is in fast exchange with respect to conformational equilibrium that is manifest for the protein without the ligand.

Several physicochemical parameters, such as buffer, pH, ionic strength, addition of osmolytes, etc., were varied in an attempt to improve the NMR spectral characteristics of IlvN to render it amenable for structural characterization. However, these were met with no success. Unfortunately, even perdeuteration of IlvN did not yield the desired effect, further supporting the notion of differences in conformation between the valine-bound and free states. Despite the limitations, we have been able to infer certain important structural features of the ligand free state.

In what follows, we describe the results of the studies of the structural characterization of IlvN-V and contrast the results with the known properties of IlvN.

Structure Determination. Sequence specific resonance assignments[46] have shown that IlvN-V exists as a single species in solution. A single set of resonances was observed for all NMR active backbone and side chain nuclei. Figure 3 shows the sequence specifically assigned $^{1}H-^{15}N$ correlation spectrum of IlvN-V.

Secondary Structure. Assignment of sequential and medium-range NOEs showed that each protomer was composed of three α-helices and four β-strands, viz., helix α1 (M24−R34), helix α2 (L64−D72), helix α3 (T88−F96), strand β1 (N10−R18), strand β2 (G40−I46), strand β3 (K51−N59), and strand β4 (V77−N83). Figure 4A shows the NOE connectivity for residues in helix 1. These results were in good agreement with the secondary structure determined from chemical shifts. The summary of the observed sequential and medium-range NOEs is shown in Figure S-4 of the Supporting Information.

Tertiary Structure. The tertiary structure of IlvN-V was determined using NMR-derived distance, dihedral angle, and hydrogen bond restraints. A total of 2770 unambiguous distance restraints were obtained from assignment of NOEs between pairs of mutually cross-relaxing pairs of protons or groups of protons, as identified in the ^{13}C-edited and ^{15}N-edited three-dimensional NOESY spectra. An additional 136 hydrogen bond distance restraints were introduced to restrain backbone hydrogen bond donor−acceptor pairs within regular secondary structural elements. A total of 364 backbone ϕ and ψ dihedral angle restraints, which were consistent with the sequential NOE patterns, were included in the structure calculation protocols. As mentioned above, gel filtration studies had shown that IlvN-V exists as a dimer. Unfortunately, attempts to prepare isotopically asymmetrically labeled samples of IlvN-V were not successful because the molecule was not stable to denaturation−renaturation procedures that were necessary to produce such samples. Because of the fast exchange of valine, it was not possible to observe NOEs between protein and ligand. In light of this, it must be noted that all NOEs identified, including intersubunit NOEs, were those assigned in spectra of uniformly labeled samples. In the initial rounds of structure calculation, the tertiary structure of IlvN-V was determined on the basis of unambiguously identified intrasubunit NOEs. In each protomer, the four strands form a central antiparallel β-sheet that is sandwiched between helices α1 and α2 on one face and helix α3, the C-terminal helix, on the opposite face. The first two helices are amphipathic in nature and are packed against the β-sheet. The third helix extends to the penultimate residue of the protein and makes contact with strands β2 and β3. The protomer adopts the ferrodoxin-like fold with a $\beta\alpha\beta\beta\alpha\beta$ topology complemented by a C-terminal helix.

Quaternary Structure. Figure 4B shows the pattern of NOEs observed for the residues in strand β2. Correlations observed between amide protons of G40 and L57, L42 and W55, and L44 and H53 are intrasubunit, cross-strand NOEs between residues in strands β2 and β3. In contrast, the NOE correlation between amide protons of I41 and C43 is a clear indication that

dx.doi.org/10.1021/bi301415m | Biochemistry 2013, 52, 70−83

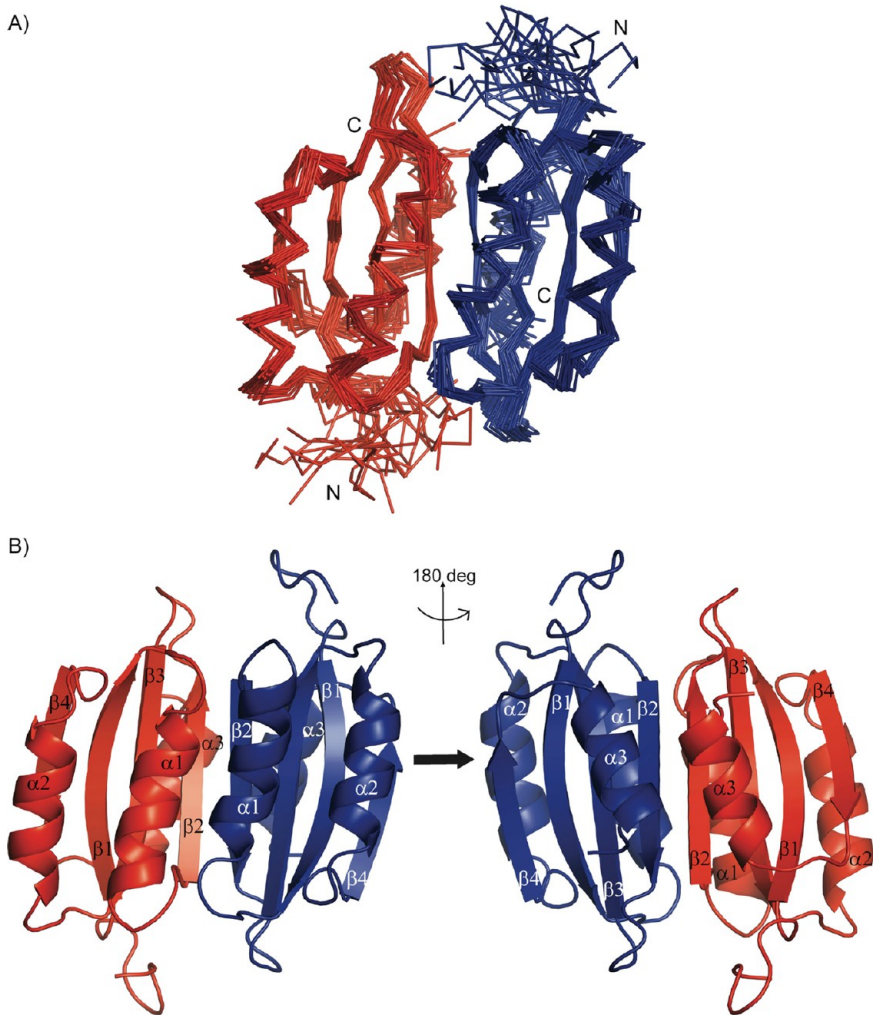

Figure 5. (A) Superposition of the ensemble of 20 low-energy structures of IlvN-V in ribbon representation. When superposed on backbone N, C^{α}, and C′ atoms of residues 10−96, the ensemble shows a pairwise rmsd of 0.73 Å. (B) Cartoon representation of the lowest-energy structure of IlvN-V. The two faces of the protein are shown. The structure is characterized by an eight-stranded central β-sheet that is sandwiched by helices on both faces.

Table 2. Comparison[a] of the Secondary Structures of IlvN-V and IlvH[b]

secondary structure	IlvN-V	no. of residues in secondary structure	IlvH	no. of residues in secondary structure
β1	N10−R18	9	R2−E10	9
α1	M24−R34	11	A15−S24	10
β2	G40−I46	7	I30−P37	8
β3	K51−N59	9	L43−V51	9
α2	L64−D72	9	V56−H65	10
β4	V77−N83	7	V70−E75	6
α3	T88−F96	9	–	–

[a]Comparisons were drawn from the results of the structural alignment of the protein using the DALI server. [b]Residues 1−76 in IlvH.

the two subunits associate via the complementary β2 strands in an antiparallel manner. A schematic representation of these NOEs is shown in Figure 4C. NOEs identified between residues in helix α1 of each protomer provided further proof that the subunits are oriented in an antiparallel manner. H−D exchange studies performed on the valine-bound form supported this β-strand registry. Of the two edge strands, β2 and β4, in each protomer, only the amide protons of residues in the β4 strand showed rapid exchange, indicating that they were solvent-exposed. In contrast, amide protons of residues in strand β2 were slow to exchange, indicating that they were well protected from bulk solvent (Figure S-5 of the Supporting Information). A total of 38 NOE and 8 hydrogen bond distance restraints were introduced for calculation of the quaternary structure of IlvN-V. Table 1 lists the type and number of restraints used for structure determination. The table also lists structural parameters derived for the 20 lowest-energy structures. Figure 5A shows a superposition of the 20 low-energy structures. When superposed on the backbone N, C^{α}, and C′ atoms, the ensemble of structures shows a root-mean-square deviation (rmsd) of 0.73 ± 0.13 Å, indicating that the structures have been determined to good precision. The ensemble of structures showed an rmsd of 1.16 ± 0.13 Å when superposed on all heavy atoms. N-Terminal residues 1−8 are ill defined because of a lack of restraints and are excluded from the analysis. The lowest-energy structure is shown in cartoon representation in Figure 5B. The ensemble of structures were of good stereochemical quality as 88.4, 10.4, and 1.2% of the backbone dihedral angles lay in the most favored, additionally allowed, and generously allowed regions of the Ramachandran map,[47] respectively (Figure S-6 of the Supporting Information).

dx.doi.org/10.1021/bi301415m | *Biochemistry* 2013, 52, 70−83

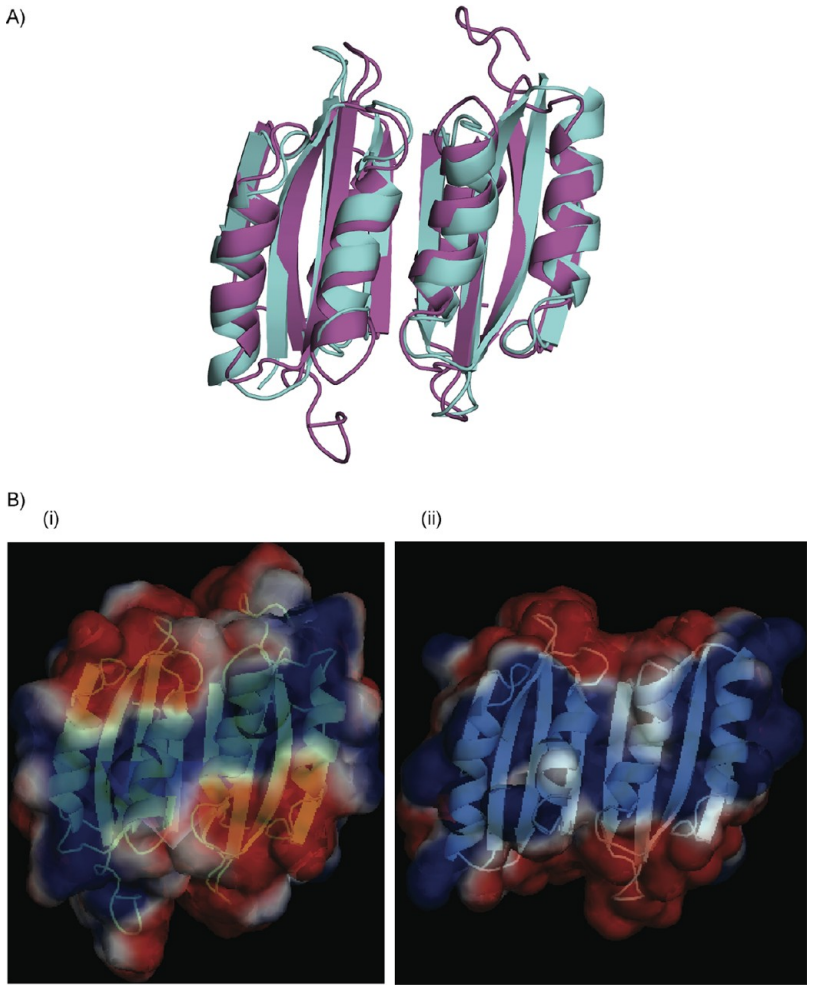

Figure 6. (A) Superposition of the ACT domain of IlvH [residues 1−76 (PDB entry 2F1F)] onto IlvN-V. IlvH is colored cyan and IlvN-V magenta. The conservation of structure is remarkable given that the sequences are only 30% identical and that IlvH is in the unbound state. Differences in the conformation of the loop structures may be due to the inherent flexibility of these regions of the protein in solution. (B) Electrostatic surface potential of (i) IlvN-V and (ii) IlvH [residues 1−76 (PDB entry 2F1F)]. The surface potentials were calculated using the APBS[59] and PDB2PQR[60,61] tools in PyMOL. A prominent positively charged surface is observed for both proteins. The surface shown here is the one that is thought to be crucial for interaction with the CSU.

In the dimer, the two protomers are arranged in an antiparallel fashion and are related by a 2-fold axis of symmetry. The dimerization occurs through the hydrophobic face containing strand β2 and helices α1 and α3 of the protomer. In IlvN-V, an eight-stranded antiparallel β-sheet at the core is flanked by four α-helices on one face and two α-helices on the other. The dimer interface is stabilized by main chain hydrogen bonds mainly across the β2 strands from each monomer and side chain nonbonded interactions across the respective helices. The interface encloses a buried surface area of 2837 Å^2. Dimerization results in the formation of the ACT domain, a conserved fold that is found in enzymes that function in metabolic pathways and in certain transcription factors.[25] The principal role of the ACT domain is a regulatory one, generally feedback inhibition, which is precipitated by binding effector molecules. In the case of IlvN, the effector molecules are the amino acids valine and isoleucine but not leucine, which are the end products of the metabolic pathway. As mentioned above, the binding to either valine or isoleucine causes significant changes in the conformational properties of IlvN.

Comparison with IlvH. IlvN shares significant sequence and structural homology with the N-terminal domain (ACT domain) of IlvH, the RSU of *E. coli* AHAS III. These two proteins share 30% identical sequences in these regions. The structure of IlvH in the unliganded state was determined by X-ray crystallography to a resolution of 1.75 Å.[14] IlvH is a homodimer with two domains of similar size, the N-terminal and the C-terminal domain, both adopting the ferrodoxin fold. The N- and C-terminal domains are at right angles to each other in an L-shaped conformation. The secondary structural elements (Table 2) in the ACT domains of IlvH and IlvN are identical ($\beta\alpha\beta\beta\alpha\beta$ topology). This is surprising because the structure of IlvH is that of the protein in the unliganded state. The tertiary structures of these two proteins superpose remarkably well, with an rmsd of 1.4 Å, when superposed on the backbone C$^\alpha$ atoms of residues in well-defined secondary structural regions of the proteins (Figure 6A). When superposed on all the C$^\alpha$ atoms within this ACT domain, the molecules exhibit an rmsd of 2.4 Å. This larger deviation arises mainly from the conformational flexibility observed for the loop regions of IlvN-V.

Figure 6B shows the electrostatic surface potential for the ACT domain of IlvN-V and IlvH. The view shown here is of the common helical surface of the two proteins that are thought to interact with the CSUs.[18] IlvH possesses a larger area of positive

dx.doi.org/10.1021/bi301415m | *Biochemistry* 2013, 52, 70−83

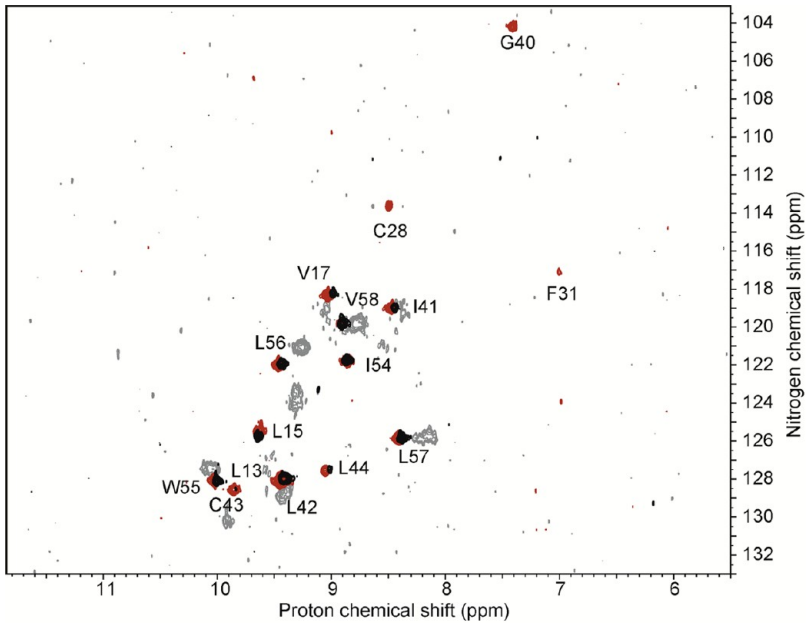

Figure 7. Overlay of two-dimensional $^{1}H-^{15}N$ HSQC spectra recorded to monitor H−D exchange rates in IlvN and IlvN-V. The spectrum of IlvN is colored gray. The spectrum of IlvN-V is colored red. The spectrum colored black was obtained by addition of 5 mM valine (in D_2O) to the sample of IlvN, whose spectrum is colored gray. The total acquisition time of each spectrum was 24 h.

charge, whereas in IlvN-V, a narrow band of positive charge extends diagonally across the surface. These differences in electrostatic potential could play a critical role in determining the affinity of interaction between RSUs and CSUs from different isozymes.

Solution Structure of IlvN. Although we have not been able to determine the structure of IlvN, several aspects of the structure of the ligand free form were understood by comparison of H−D exchange NMR spectra and other physicochemical properties of the protein in the two states.

Hydrogen−Deuterium Exchange Studies. Hydrogen−deuterium exchange studies provide critical information about the structural milieu of exchangeable protons in proteins. In general, those protons that are either buried in the protein interior or are strongly hydrogen bonded exchange at a slow rate.

Figure 7 shows an overlay of the two-dimensional proton−nitrogen correlation spectra of IlvN and IlvN-V in D_2O. In IlvN-V, the residues whose backbone amides were protected from solvent exchange after incubation in D_2O for a period of 24 h were L13, L15, V17, C28, F31, G40, I41, L42, C43, L44, I54, W55, L56, L57, and V58. In the case of IlvN, some of the amides are also resistant to exchange. Because of the large conformational differences between these two states, the spectra do not superpose, precluding a transfer of assignments from one form to the other. Addition of valine to this solution of IlvN resulted in a spectrum (black) that provided an answer to the identity of these residues. Thus, the residues in IlvN that remained unexchanged were L13, L15, V17, I41, L42, C43, L44, I54, W55, L56, L57, and V58, the majority of which were protected in the valine-bound form too. These residues are present in strands β1 and β3 and importantly in strand β2, which is at the dimer interface. This unequivocally establishes that (a) the central β-sheet is intact in IlvN, (b) the strand registry is maintained in both IlvN and IlvN-V, and (c) the conformational change or switch in converting from the ligand free to the ligand-bound form does not involve changes in the β-sheet topology.

On the other hand, it is clear that the residues in helices 2 and 3 of IlvN-V exchange over the same time period. In contrast, the amide protons of residues C28 and F31 in helix 1 are solvent-protected in IlvN-V but appear to be solvent-exposed in IlvN, suggesting that the residues in helix 1 are involved in valine binding or are dynamic in the unbound form.

Alkylation Studies of the Cysteine Residues. Analysis of the surface accessibility calculations of the residues of IlvN-V showed that the two cysteines, viz., C28 and C43, were buried. C28 is a part of helix α1 and C43 a part of strand β2, and both are present at the dimer interface. Figure 8 shows the mass spectra of IlvN that were subjected to alkylation reaction. In the case of IlvN, alkylation of cysteine residues occurs rapidly (<5 min), whereas the cysteines in IlvN-V are resistant to chemical modification over the same time interval. A similar effect is also observed in the case of IlvN-I. This is a clear indication that the cysteines in IlvN are solvent-exposed. H−D exchange studies have already shown that the helical segments in IlvN are dynamic. We suggest that the helices in IlvN undergo a coil-to-helix transition in going from the ligand free to the ligand-bound form. It is interesting to note that alkylation reactions conducted over longer time periods, in the presence of the ligand, also result in chemical modification of the protein, indicating that the protein is dynamic in either state (data not shown).

Isoleucine Binding Studies of IlvN. In a manner similar to that used for valine, addition of isoleucine also causes significant narrowing of resonance lines in the NMR spectrum of IlvN. However, the dissociation constant for isoleucine is significantly higher.[3] Figure 9A shows the superposition of $^{1}H-^{15}N$ HSQC spectra of IlvN-V and IlvN-I. While differences in chemical shifts for a large number of residues can be observed (Figure S-7 of the Supporting Information), the similarity of the spectrum leads us to believe that the structure of IlvN in the presence of valine or isoleucine is similar. These differences in chemical shifts may be an indicator of the differences in conformational exchange properties of IlvN depending on the specific branched chain amino acid with which it interacts.

dx.doi.org/10.1021/bi301415m | *Biochemistry* 2013, 52, 70−83

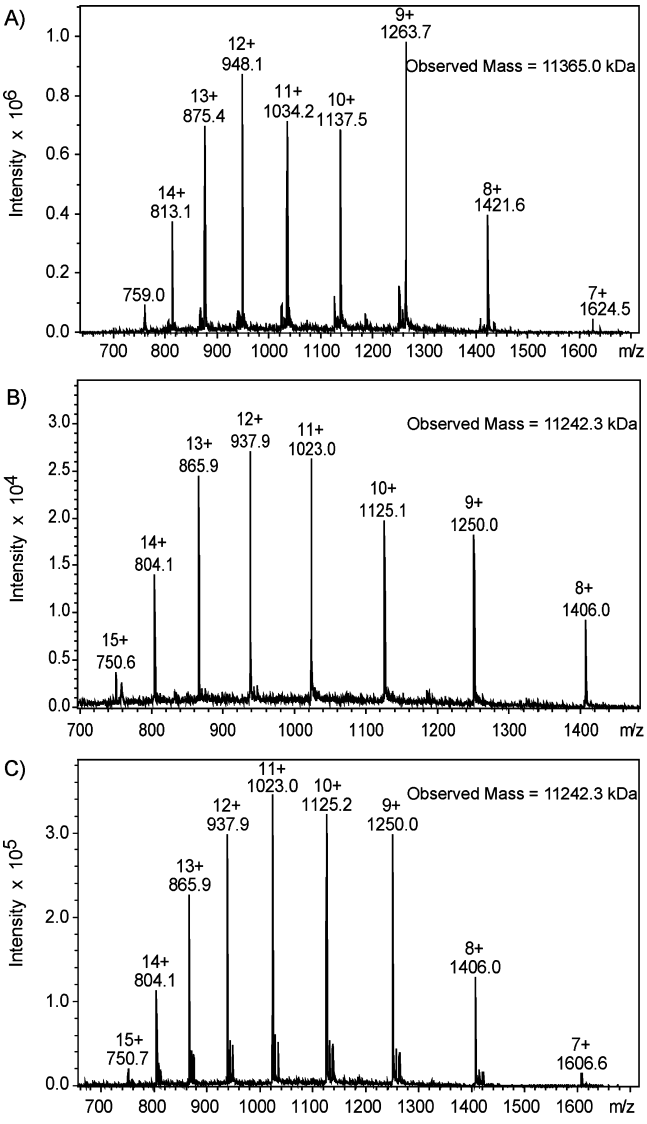

Figure 8. LC-ESI mass spectra of (A) IlvN, (B) IlvN-V, and (C) IlvN-I after chemical modification reactions conducted using iodoacetamide as the cysteine-modifying agent. Native IlvN has a calculated mass of 11250 Da. The increase in mass of unliganded IlvN (58 × 2 Da) clearly shows that both cysteines are modified within 5 min of the start of the reaction. Minor peaks in the spectrum corresponding to the unmodified protein can also be observed. For the same time period, IlvN-V is unmodified. In the case of IlvN-I, the great majority of the protein exists as the unmodified species. Correspondingly, minor peaks arising from the singly and doubly alkylated protein can also be observed. Differences between observed and calculated masses in the case of IlvN-V and IlvN-I are caused by hardware errors in the instrument.

Estimates of changes in chemical shifts between the two states were also made by monitoring the changes in chemical shifts of a sample of IlvN-I upon addition of valine. Residues showing a chemical shift perturbation greater than the average (of 0.05 ppm) were identified as shown in Figure 9B. These were L15, N19, V23, V27, C28, G29, A32, N37, E39, G40, I41, C43, L44, I46, S52, H53, I54, L56, D60, R63, V95, F96, and Q98. It was also observed that the chemical shifts for the three initial residues of helix α1, viz., M24, T25, and H26, were either absent or significantly shifted in the $^{1}H-^{15}N$ HSQC spectrum. Once again, the residues that exhibit large chemical shift changes are ones that occur at the dimer interface. The data suggest that the amino acid binding pocket is located at or near the dimer interface and corroborates the model suggested by Kaplun et al.[14]

DISCUSSION

AHAS is a unique multisubunit enzyme, which is allosterically regulated by the end products of the metabolic pathway in which it participates. Many of the enzymes that function in primary metabolic pathways as also transcription factors possess independently folded domains, known as ACT domains that are responsible for this regulatory function. Unlike the *E. coli* AHAS III RSU, viz., IlvH, the *E. coli* AHAS I RSU, i.e., IlvN, forms an independently folded ACT domain and thus should be termed the ACT subunit. Thus far, structural characterization of ACT domains has been accomplished by X-ray crystallography.[48−52] Here, we have conducted the structural characterization of an ACT subunit using solution NMR methods complemented with circular dichroic and mass spectrometric studies to show that this ACT subunit exhibits dynamic and motional properties that provide an understanding of the structure and function of the AHAS holoenzyme. The NMR spectral properties of unliganded IlvN indicate that this molecule exists in a mixed population of conformational states. These conformational states are in dynamic equilibrium and are undergoing exchange at a rate that is intermediate on the NMR time scale. The significant broadening of lines observed in the case of IlvN is strong evidence of this rate of exchange. The low resolution of the spectra makes it difficult to ascertain the number of species that exist. Conformational exchange has its origins in specific structural transitions. Proline cis−trans isomerization (bond rotation isomerization) as observed in the case of the AHSP protein,[53] prosthetic group exchange reactions as observed in the case of *b*-type heme proteins,[54,55] and holo-acyl carrier protein[56] are well-documented sources of conformational exchange observed in these proteins. In the case of multimeric proteins, the existence of an equilibrium between monomeric and multimeric or between multimeric species could also be a source of the observed conformational exchange. In the case of IlvN, while one cannot rule out the possibility of a monomer−dimer equilibrium, it is certainly not the main source of the observed line broadening effect in the ACT subunit. Evidence of this comes from the hydrogen−deuterium exchange studies, which indicate that the amide protons on strand β2 undergo slow exchange with bulk solvent under all the experimental conditions explored here, indicating that these amide protons are strongly hydrogen bonded, which is the case when the molecule exists as a dimer. The residues on strand β4 on the other hand exchange with bulk solvent quickly. This suggests that the central eight-stranded β-sheet is intact even in the absence of valine. On the other hand, the residues in the helical regions appear to exchange between coil-like conformations. Thus, it is the helices in the ACT subunit that are disordered, of which helices 1 and 3 are at the dimer interface. Interestingly, addition of valine causes a significant change in the spectral properties as well as in the structure of the molecule. Here the protein undergoes a remarkable coil-to-helix transition. Whether this results from a population shift between conformers or from folding, nucleated by binding valine, i.e., an induced fit mechanism, is difficult to establish at this stage. When valine binds, a single set of resonances is observed for the residues in the protein. This indicates that the rate of transition between conformational states migrates either into the fast exchange regime or into the slow exchange regime, where the minor populations are below the detectable limit of the NMR methods

dx.doi.org/10.1021/bi301415m | *Biochemistry* 2013, 52, 70−83

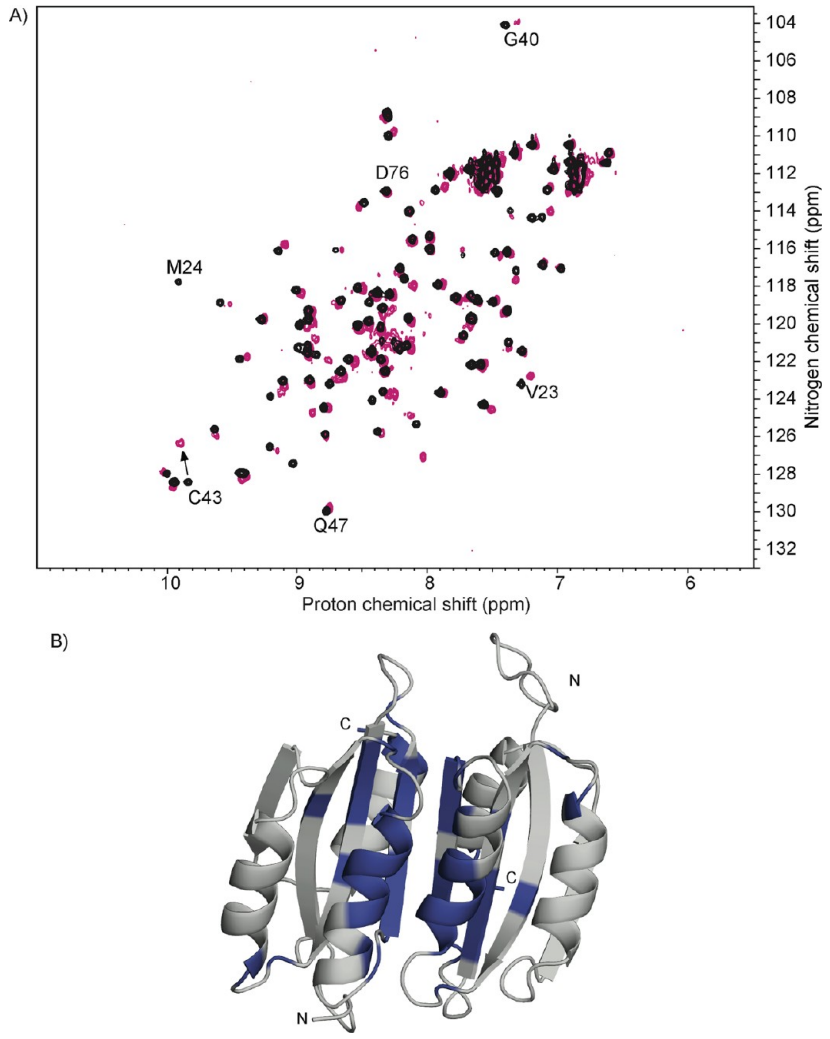

Figure 9. (A) Overlay of the $^{1}H-^{15}N$ HSQC spectra of IlvN-V (black) and IlvN-I (magenta). Spectra were recorded at valine and isoleucine concentrations of 5 and 10 mM, respectively. Similarity in the spectra of IlvN in the presence of valine and isoleucine indicates that the structure of the molecule is similar in the presence of either ligand. (B) Residues in IlvN-I that show significant chemical shift perturbation upon addition of valine are indicated on the structure of IlvN-V. A significant proportion of the residues that are perturbed are at the dimer interface. This may due to the higher affinity for valine, coupled with large conformational changes.

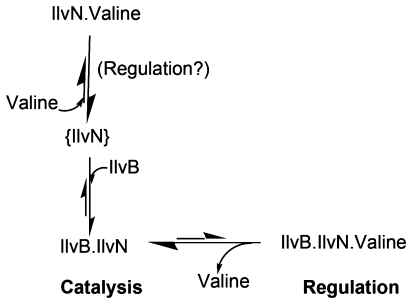

Figure 10. Schematic representation of the conformational equilibria exhibited by IlvN. In this scheme, IlvN exists as a mixture of conformational states in the free form. At low valine concentrations, the equilibrium is shifted toward formation of the CSU·RSU complex, and this results in catalysis. High valine concentrations result in allosteric regulation of the AHAS enzyme.

applied here. Additional evidence of this coil-to-helix transition comes from the chemical modification reactions of the cysteine thiols. The fact that IlvN undergoes facile alkylation in the absence of valine is indicative of the fact that the cysteine thiols are solvent-exposed. However, in IlvN-V, these cysteines are buried and continue to exist in the reduced form. Evidence of this comes from the $^{13}C^{\beta}$ chemical shifts for these cysteines.

This disordered to helix transition may be vital in the mechanism of activation and/or regulation of AHAS activity. Chipman and co-workers have indicated that the IlvB·IlvN complex is in slow exchange and that this complex does not dissociate upon valine binding.[18] Our studies have shown that IlvN can exist as a stable entity in solution in the absence of either the CSU or valine. Importantly, valine binding to this free form causes a conformational change. Additionally, the off rate for valine is fast compared to the protein conformational exchange rate. Thus, valine could partition between the IlvB·IlvN complex and free IlvN depending on the threshold concentration of valine and the relative dissociation rates for the individual complexes. These possibilities are schematically represented in Figure 10. It is not known whether binding of valine to free IlvN results in regulation.

It has been suggested that the surface formed from helices α1 and α2, which is common to all the regulatory subunits of *E. coli* AHAS isozymes, may be important for interaction with the

dx.doi.org/10.1021/bi301415m | *Biochemistry* 2013, 52, 70−83

catalytic subunits, and this may explain the origin of cross activation of CSUs by RSUs from different AHASs.[18] The similarity in surface charge is another strong indicator of the ability of the ACT domain of IlvH in cross-activating IlvB. Furthermore, Kaplun et al. have noted that the temperature factors for the two helices in the N-terminal ACT domain of IlvH, which correspond to helices I and II of IlvN, are unusually high.[14] It has also been observed that in NikR, a transcription factor that contains a regulatory ACT domain, a similar coil-to-helix transition takes place upon the protein binding Ni^{2+}.[49,57] This structural stabilization is thought to be vital for the binding of DNA by NikR.[58] Thus, it could be rationalized that the valine insensitive mutant forms of IlvN[16] are those that impose restrictions on conformational flexibility, either toward valine binding or on the above-mentioned coil-to-helix transitions.

It is important to note that the structure of IlvH is in the unliganded state, yet the ACT domains in IlvH and IlvN are seemingly identical. It has been shown that the ACT domain of IlvH is sufficient for activation of catalysis but is not sensitive to valine inhibition.[13] The residues directly interacting with valine are known to be in this ACT domain. The additional C-terminal domain is purported to be required to stabilize the dimer conformation necessary for valine binding and sensitivity.[15] The effect of the C-terminal domain on the conformation and flexibility of the ACT domain of IlvH has not been characterized. However, it is clear that the inherent conformational flexibility may be a prerequisite for activating the holoenzyme, and this could partially explain the observed nonspecific activation between the subunits, without the C-terminal domain.

The question of the subunit composition in the AHAS holoenzyme remains to be answered. It is clear that IlvN and IlvN-V are dimeric in solution. It is thus reasonable to assume that it is this dimeric form of IlvN that will interact and activate IlvB. From symmetry considerations, the stoichiometry of RSUs and CSUs in the AHAS I holoenzyme will in all probability be in the ratio of 4:4.

Another aspect of the AHAS I holoenzyme that is not understood is the nature of the interaction between the RSU and CSU. Determination of the structure of IlvN in the holoenzyme presents a formidable challenge given the overall size of the complex. Chipman and co-workers have earlier shown that *E. coli* AHAS I follows the classical M−W−C model of allosteric regulation.[10] In solution, IlvN clearly undergoes conformational exchange. An induced fit response can also be observed upon binding valine. Will the binding of IlvN to IlvB be governed by either conformational selection, induced fit, or both? It is unfortunate that attempts to crystallize the AHAS I holoenzyme have met with little success. It is clear that parameters such as dissociation constants and, as shown here, conformational exchange and folding will govern the level of detail to which the structure of the complex may be determined.

In conclusion, we have determined the structure of IlvN in the valine-bound state. The dissociation constant for the binding of valine to IlvN has also been experimentally verified. An important outcome of this study is the demonstration that free IlvN exists in solution as an equilibrium mixture of two or more conformational states. There is a significant conformational change induced in IlvN upon binding the allosteric regulators valine and isoleucine, which are the end products of the branched chain amino acid biosynthesis pathway. The amino acid leucine does not elicit similar conformational changes in the same concentration range. Binding of valine induces coil-to-helix transitions. These reversible conformational changes are essential for the function of IlvN as an activator of the catalytic subunit and in the allosteric regulation of AHAS's activity.

■ ASSOCIATED CONTENT

Supporting Information

Figures providing corroborative evidence for the data shown in this paper. This material is available free of charge via the Internet at http://pubs.acs.org.

Accession Codes

The structural coordinates for the 20 low-energy structures of IlvN-V have been deposited in the Protein Data Bank as entry 2LVW. The chemical shift assignments for IlvN-V have been deposited in the Biological Magnetic Resonance Bank as entry 16687.

■ AUTHOR INFORMATION

Corresponding Author

*Molecular Biophysics Unit, Indian Institute of Science, Bangalore 560012, Karnataka, India. Telephone: 91 80 2293 2839. Fax: 91 80 2360 0535. E-mail: sidd@mbu.iisc.ernet.in.

Funding

N.M.K. is grateful to the Council for Scientific and Industrial Research for the Senior Research Fellowship.

Notes

The authors declare no competing financial interest.

■ ACKNOWLEDGMENTS

We thank the Department of Science and Technology and the Department of Biotechnology for the NMR and Mass Spectrometric Facilities at the Indian Institute of Science.

■ ABBREVIATIONS

AHAS, acetohydroxyacid synthase; RSU, regulatory subunit; CSU, catalytic subunit; IlvN-V, IlvN-valine; IlvN-I, IlvN-isoleucine; IlvN-L, IlvN-leucine; TPP, thiamine pyrophosphate; FAD, flavin adenine dinucleotide; EDTA, ethylenediaminetetraacetic acid; DSS, sodium 4,4-dimethyl-4-silapentane sulfonate; FPLC, fast protein liquid chromatography; LC−ESI-MS, liquid chromatography and electrospray ionization mass spectrometry; HPLC, high-performance liquid chromatography; ITC, isothermal titration calorimetry; H−D, hydrogen−deuterium; HSQC, heteronuclear single-quantum coherence; NOE, nuclear Overhauser effect; NOESY, nuclear Overhauser effect exchange spectroscopy; PDB, Protein Data Bank.

■ REFERENCES

(1) Umbarger, H. E. (1987) Biosynthesis of Branched-Chain Amino Acids. In *Escherichia coli and Salmonella typhimurium: Cellular and Molecular Biology* (Neidhardt, F. C., Ed.) pp 352−367, American Society for Microbiology, Washington DC.

(2) Chipman, D. M., Duggleby, R. G., and Tittmann, K. (2005) Mechanisms of acetohydroxyacid synthases. *Curr. Opin. Chem. Biol. 9*, 475−481.

(3) McCourt, J. A., and Duggleby, R. G. (2006) Acetohydroxyacid synthase and its role in the biosynthetic pathway for branched-chain amino acids. *Amino Acids 31*, 173−210.

(4) Lawther, R. P., Wek, R. C., Lopes, J. M., Perira, R., Taillon, B. E., and Wesley, G. (1987) The complete nucleotide sequence of the ilvGMEDA Operon of *Escherichia coli* K-12. *Nucleic Acids Res. 15*, 2137−2155.

(5) Squires, C. H., DeFelice, M., Devereux, J., and Calvo, J. M. (1983) Molecular structure of ilvIH and its evolutionary relationship to ilvG in *Escherichia coli* K12. *Nucleic Acids Res. 11*, 5299−5313.

(6) Wek, R. C., Hauser, C. A., and Hatfield, G. W. (1985) The nucleotide sequence of the ilvBN operon of *Escherichia coli*: Sequence homologies of the acetohydroxy acid synthase isozymes. *Nucleic Acids Res. 13*, 3995−4010.
(7) Pang, S. S., and Duggleby, R. G. (1999) Expression, purification, characterization, and reconstitution of the large and small subunits of yeast acetohydroxyacid synthase. *Biochemistry 38*, 5222−5231.
(8) Lee, Y. T., and Duggleby, R. G. (2001) Identification of the regulatory subunit of *Arabidopsis thaliana* acetohydroxyacid synthase and reconstitution with its catalytic subunit. *Biochemistry 40*, 6836−6844.
(9) Hill, C. M., Pang, S. S., and Duggleby, R. G. (1997) Purification of *Escherichia coli* acetohydroxyacid synthase isoenzyme II and reconstitution of active enzyme from its individual pure subunits. *Biochem. J. 327* (Part 3), 891−898.
(10) Vinogradov, V., Vyazmensky, M., Engel, S., Belenky, I., Kaplun, A., Kryukov, O., Barak, Z., and Chipman, D. M. (2006) Acetohydroxyacid synthase isozyme I from *Escherichia coli* has unique catalytic and regulatory properties. *Biochim. Biophys. Acta 1760*, 356−363.
(11) Vyazmensky, M., Sella, C., Barak, Z., and Chipman, D. M. (1996) Isolation and characterization of subunits of acetohydroxy acid synthase isozyme III and reconstitution of the holoenzyme. *Biochemistry 35*, 10339−10346.
(12) Mendel, S., Elkayam, T., Sella, C., Vinogradov, V., Vyazmensky, M., Chipman, D. M., and Barak, Z. (2001) Acetohydroxyacid synthase: A proposed structure for regulatory subunits supported by evidence from mutagenesis. *J. Mol. Biol. 307*, 465−477.
(13) Mendel, S., Vinogradov, M., Vyazmensky, M., Chipman, D. M., and Barak, Z. (2003) The N-terminal domain of the regulatory subunit is sufficient for complete activation of acetohydroxyacid synthase III from *Escherichia coli*. *J. Mol. Biol. 325*, 275−284.
(14) Kaplun, A., Vyazmensky, M., Zherdev, Y., Belenky, I., Slutzker, A., Mendel, S., Barak, Z., Chipman, D. M., and Shaanan, B. (2006) Structure of the regulatory subunit of acetohydroxyacid synthase isozyme III from *Escherichia coli*. *J. Mol. Biol. 357*, 951−963.
(15) Slutzker, A., Vyazmensky, M., Chipman, D. M., and Barak, Z. (2011) Role of the C-terminal domain of the regulatory subunit of AHAS isozyme III: Use of random mutagenesis with in vivo reconstitution (REM-ivrs). *Biochim. Biophys. Acta 1814*, 449−455.
(16) Barak, Z., and Chipman, D. M. (2012) Allosteric regulation in acetohydroxyacid synthases (AHASs): Different structures and kinetic behavior in isozymes in the same organisms. *Arch. Biochem. Biophys. 519*, 167−174.
(17) Lee, Y. T., and Duggleby, R. G. (2000) Mutagenesis studies on the sensitivity of *Escherichia coli* acetohydroxyacid synthase II to herbicides and valine. *Biochem. J. 350* (Part 1), 69−73.
(18) Vyazmensky, M., Zherdev, Y., Slutzker, A., Belenky, I., Kryukov, O., Barak, Z., and Chipman, D. M. (2009) Interactions between large and small subunits of different acetohydroxyacid synthase isozymes of *Escherichia coli*. *Biochemistry 48*, 8731−8737.
(19) Pang, S. S., Duggleby, R. G., and Guddat, L. W. (2002) Crystal structure of yeast acetohydroxyacid synthase: A target for herbicidal inhibitors. *J. Mol. Biol. 317*, 249−262.
(20) McCourt, J. A., Pang, S. S., King-Scott, J., Guddat, L. W., and Duggleby, R. G. (2006) Herbicide-binding sites revealed in the structure of plant acetohydroxyacid synthase. *Proc. Natl. Acad. Sci. U.S.A. 103*, 569−573.
(21) McCourt, J. A., Pang, S. S., Guddat, L. W., and Duggleby, R. G. (2005) Elucidating the specificity of binding of sulfonylurea herbicides to acetohydroxyacid synthase. *Biochemistry 44*, 2330−2338.
(22) Pang, S. S., Guddat, L. W., and Duggleby, R. G. (2003) Molecular basis of sulfonylurea herbicide inhibition of acetohydroxyacid synthase. *J. Biol. Chem. 278*, 7639−7644.
(23) Wang, J. G., Lee, P. K., Dong, Y. H., Pang, S. S., Duggleby, R. G., Li, Z. M., and Guddat, L. W. (2009) Crystal structures of two novel sulfonylurea herbicides in complex with *Arabidopsis thaliana* acetohydroxyacid synthase. *FEBS J. 276*, 1282−1290.
(24) Petkowski, J. J., Chruszcz, M., Zimmerman, M. D., Zheng, H., Skarina, T., Onopriyenko, O., Cymborowski, M. T., Koclega, K. D., Savchenko, A., Edwards, A., and Minor, W. (2007) Crystal structures of TM0549 and NE1324: Two orthologs of *E. coli* AHAS isozyme III small regulatory subunit. *Protein Sci. 16*, 1360−1367.
(25) Grant, G. A. (2006) The ACT domain: A small molecule binding domain and its role as a common regulatory element. *J. Biol. Chem. 281*, 33825−33829.
(26) Liberles, J. S., Thorolfsson, M., and Martinez, A. (2005) Allosteric mechanisms in ACT domain containing enzymes involved in amino acid metabolism. *Amino Acids 28*, 1−12.
(27) Aravind, L., and Koonin, E. V. (1999) Gleaning non-trivial structural, functional and evolutionary information about proteins by iterative database searches. *J. Mol. Biol. 287*, 1023−1040.
(28) Mitra, A., and Sarma, S. P. (2008) *Escherichia coli* ilvN interacts with the FAD binding domain of ilvB and activates the AHAS I enzyme. *Biochemistry 47*, 1518−1531.
(29) Karanth, N. M., Mitra, A., and Sarma, S. P. (2009) Solution NMR studies of acetohydroxy acid synthase I: Identification of the sites of inter-subunit interactions using multidimensional NMR methods. *J. Mol. Catal. B: Enzym. 61*, 7−13.
(30) Piotto, M., Saudek, V., and Sklenar, V. (1992) Gradient-tailored excitation for single-quantum NMR spectroscopy of aqueous solutions. *J. Biomol. NMR 2*, 661−665.
(31) Mori, S., Abeygunawardana, C., Johnson, M. O., and van Zijl, P. C. (1995) Improved sensitivity of HSQC spectra of exchanging protons at short interscan delays using a new fast HSQC (FHSQC) detection scheme that avoids water saturation. *J. Magn. Reson., Ser. B 108*, 94−98.
(32) Vuister, G. W., and Bax, A. (1992) Resolution Enhancement and Spectral Editing of Uniformly ^{13}C-Enriched Proteins by Homonuclear Broadband ^{13}C Decoupling. *J. Magn. Reson. 98*, 428−435.
(33) Marion, D., Kay, L. E., Sparks, S. W., Torchia, D. A., and Bax, A. (1989) Three-Dimensional Heteronuclear NMR of ^{15}N-Labeled Proteins. *J. Am. Chem. Soc. 111*, 1515−1517.
(34) Delaglio, F., Grzesiek, S., Vuister, G. W., Zhu, G., Pfeifer, J., and Bax, A. (1995) NMRPipe: A multidimensional spectral processing system based on UNIX pipes. *J. Biomol. NMR 6*, 277−293.
(35) Kraulis, P. J., Domaille, P. J., Campbell-Burk, S. L., Van Aken, T., and Laue, E. D. (1994) Solution structure and dynamics of ras p21·GDP determined by heteronuclear three- and four-dimensional NMR spectroscopy. *Biochemistry 33*, 3515−3531.
(36) Kraulis, P. J. (1989) ANSIG: A Program for the Assignment of Protein ^{1}H 2D NMR Spectra by Interactive Graphics. *J. Magn. Reson. 84*, 627−633.
(37) Vranken, W. F., Boucher, W., Stevens, T. J., Fogh, R. H., Pajon, A., Llinas, M., Ulrich, E. L., Markley, J. L., Ionides, J., and Laue, E. D. (2005) The CCPN data model for NMR spectroscopy: Development of a software pipeline. *Proteins 59*, 687−696.
(38) Shen, Y., Delaglio, F., Cornilescu, G., and Bax, A. (2009) TALOS +: A hybrid method for predicting protein backbone torsion angles from NMR chemical shifts. *J. Biomol. NMR 44*, 213−223.
(39) Guntert, P. (1998) Structure calculation of biological macromolecules from NMR data. *Q. Rev. Biophys. 31*, 145−237.
(40) Brunger, A. T. (2007) Version 1.2 of the Crystallography and NMR system. *Nat. Protoc. 2*, 2728−2733.
(41) Brunger, A. T., Adams, P. D., Clore, G. M., DeLano, W. L., Gros, P., Grosse-Kunstleve, R. W., Jiang, J. S., Kuszewski, J., Nilges, M., Pannu, N. S., Read, R. J., Rice, L. M., Simonson, T., and Warren, G. L. (1998) Crystallography & NMR system: A new software suite for macromolecular structure determination. *Acta Crystallogr. D54*, 905−921.
(42) Bhattacharya, A., Tejero, R., and Montelione, G. T. (2007) Evaluating protein structures determined by structural genomics consortia. *Proteins 66*, 778−795.
(43) Koradi, R., Billeter, M., and Wuthrich, K. (1996) MOLMOL: A program for display and analysis of macromolecular structures. *J. Mol. Graphics 14*, 29−32 , 51−55.
(44) Holm, L., and Rosenström, P. (2010) Dali server: Conservation mapping in 3D. *Nucleic Acids Res. 38*, W545−W549.
(45) *The PyMOL Molecular Graphics System*, version 1.3r1 (2010) Schrodinger, LLC, New York.

(46) Karanth, N. M., and Sarma, S. P. (2010) ^{1}H, ^{13}C, ^{15}N assignments of the dimeric regulatory subunit (ilvN) of the *E. coli* AHAS I. *Biomol. NMR Assignments 4*, 131−133.
(47) Ramachandran, G. N., and Sasisekharan, V. (1968) Conformation of polypeptides and proteins. *Adv. Protein Chem. 23*, 283−438.
(48) Schuller, D. J., Grant, G. A., and Banaszak, L. J. (1995) The allosteric ligand site in the Vmax-type cooperative enzyme phosphoglycerate dehydrogenase. *Nat. Struct. Biol. 2*, 69−76.
(49) Schreiter, E. R., Sintchak, M. D., Guo, Y., Chivers, P. T., Sauer, R. T., and Drennan, C. L. (2003) Crystal structure of the nickel-responsive transcription factor NikR. *Nat. Struct. Biol. 10*, 794−799.
(50) Tan, K., Li, H., Zhang, R., Gu, M., Clancy, S. T., and Joachimiak, A. (2008) Structures of open (R) and close (T) states of prephenate dehydratase (PDT): Implication of allosteric regulation by L-phenylalanine. *J. Struct. Biol. 162*, 94−107.
(51) Kobe, B., Jennings, I. G., House, C. M., Michell, B. J., Goodwill, K. E., Santarsiero, B. D., Stevens, R. C., Cotton, R. G., and Kemp, B. E. (1999) Structural basis of autoregulation of phenylalanine hydroxylase. *Nat. Struct. Biol. 6*, 442−448.
(52) Mas-Droux, C., Curien, G., Robert-Genthon, M., Laurencin, M., Ferrer, J. L., and Dumas, R. (2006) A novel organization of ACT domains in allosteric enzymes revealed by the crystal structure of *Arabidopsis* aspartate kinase. *Plant Cell 18*, 1681−1692.
(53) Santiveri, C. M., Perez-Canadillas, J. M., Vadivelu, M. K., Allen, M. D., Rutherford, T. J., Watkins, N. A., and Bycroft, M. (2004) NMR structure of the α-hemoglobin stabilizing protein: Insights into conformational heterogeneity and binding. *J. Biol. Chem. 279*, 34963−34970.
(54) La Mar, G. N., Budd, D. L., Viscio, D. B., Smith, K. M., and Langry, K. C. (1978) Proton nuclear magnetic resonance characterization of heme disorder in hemoproteins. *Proc. Natl. Acad. Sci. U.S.A. 75*, 5755−5759.
(55) La Mar, G. N., Burns, P. D., Jackson, J. T., Smith, K. M., Langry, K. C., and Strittmatter, P. (1981) Proton magnetic resonance determination of the relative heme orientations in disordered native and reconstituted ferricytochrome b5. Assignment of heme resonances by deuterium labeling. *J. Biol. Chem. 256*, 6075−6079.
(56) Sharma, A. K., Sharma, S. K., Surolia, A., Surolia, N., and Sarma, S. P. (2006) Solution structures of conformationally equilibrium forms of holo-acyl carrier protein (PfACP) from *Plasmodium falciparum* provides insight into the mechanism of activation of ACPs. *Biochemistry 45*, 6904−6916.
(57) Phillips, C. M., Schreiter, E. R., Guo, Y., Wang, S. C., Zamble, D. B., and Drennan, C. L. (2008) Structural basis of the metal specificity for nickel regulatory protein NikR. *Biochemistry 47*, 1938−1946.
(58) Schreiter, E. R., Wang, S. C., Zamble, D. B., and Drennan, C. L. (2006) NikR-operator complex structure and the mechanism of repressor activation by metal ions. *Proc. Natl. Acad. Sci. U.S.A. 103*, 13676−13681.
(59) Baker, N. A., Sept, D., Joseph, S., Holst, M. J., and McCammon, J. A. (2001) Electrostatics of nanosystems: Application to microtubules and the ribosome. *Proc. Natl. Acad. Sci. U.S.A. 98*, 10037−10041.
(60) Dolinsky, T. J., Nielsen, J. E., McCammon, J. A., and Baker, N. A. (2004) PDB2PQR: An automated pipeline for the setup of Poisson−Boltzmann electrostatics calculations. *Nucleic Acids Res. 32*, W665−W667.
(61) Dolinsky, T. J., Czodrowski, P., Li, H., Nielsen, J. E., Jensen, J. H., Klebe, G., and Baker, N. A. (2007) PDB2PQR: Expanding and upgrading automated preparation of biomolecular structures for molecular simulations. *Nucleic Acids Res. 35*, W522−W525.